Two central pattern generators from the crab, *Cancer borealis*, respond robustly and differentially to extreme extracellular pH

Jessica A. Haley[†], David Hampton, Eve Marder*

Volen Center and Biology Department, Brandeis University, Waltham, MA 02454

* **Corresponding Author:**
marder@brandeis.edu

[†] **Current Address:**
Neurosciences Graduate Program, University of California San Diego, La Jolla, CA 92037

Author contributions:
Jessica A. Haley, Data curation, Formal Analysis, Investigation, Methodology, Software, Validation, Visualization, Writing – Original Draft Preparation, Writing – Review & Editing; **David Hampton**, Formal Analysis, Investigation, Writing – Original Draft Preparation, Writing – Review & Editing; **Eve Marder**, Conceptualization, Data Curation, Funding Acquisition, Project Administration, Resources, Supervision, Writing – Review & Editing

Abbreviations:
STG, stomatogastric ganglion; **CG**, cardiac ganglion; **CPG**, central pattern generator; **AB**, Anterior Burster; **PD**, Pyloric Dilator; **LP**, Lateral Pyloric; **PY**, Pyloric; **SC**, Small Cell; **LC**, Large Cell; ***lvn***, lateral ventricular nerve; **ANOVA**, analysis of variance; **PTX**, picrotoxin; **IPSP**, inhibitory post-synaptic potential; **LG**, Lateral Gastric; **MG**, Medial Gastric; **LPG**, Lateral Posterior Gastric; **GM**, Gastric Mill; **DG**, Dorsal Gastric; **AM**, Anterior Median; **Int1**, Interneuron 1; ***mvn***, medial ventricular nerve; ***dgn***, dorsal gastric nerve; ***lgn***, lateral gastric nerve; ***ion***, inferior oesophageal nerve; **IC**, Inferior Cardiac; **VD**, Ventricular Dilator; **MCN1**, Modulatory Commissural Neuron 1; **VCN**, Ventral Cardiac Neuron; **CPN2**, Commissural Projection Neuron 2; **CoG**, commissural ganglion; **KDE**, kernel density estimate; **IQR**, interquartile range; **CI**, confidence interval

Keywords: stomatogastric ganglion**,** cardiac ganglion, pyloric rhythm, crustacean, ocean acidification

Abstract

Animals and their neuronal circuits must maintain function despite significant environmental fluctuations. The crab, *Cancer borealis*, experiences daily changes in ocean temperature and pH. Here, we describe the effects of extreme changes in extracellular pH – from pH 5.5 to 10.4 – on two central pattern generating networks, the stomatogastric and cardiac ganglia of *C. borealis*. Given that the physiological properties of ion channels are known to be sensitive to pH within the range tested, it is surprising that these rhythms generally remained robust from pH 6.1 to pH 8.8. Unexpectedly, the stomatogastric ganglion was more sensitive to acid while the cardiac ganglion was more sensitive to base. Considerable animal-to-animal variability was likely a consequence of similar network performance arising from variable sets of underlying conductances. Together, these results illustrate the potential difficulty in generalizing the effects of environmental perturbation across circuits, even within the same animal.

Introduction

Nervous systems must be both robust and adaptable to changes in internal and external conditions. Many intertidal marine crustaceans, such as the crabs and lobsters inhabiting the North Atlantic, experience large fluctuations in ocean temperature, acidity, dissolved oxygen levels, and salinity. The Jonah crab, *Cancer borealis*, can often be found foraging for food in intertidal zones where it experiences temperatures between 3°C and 24°C with fluctuations as great as 10°C in a single day (Donahue et al., 2009; Haeffner Jr, 1977; Stehlik et al., 1991). As pH is temperature-dependent, ocean pH fluctuations occur over the daily, monthly, and yearly experiences of long-lived crustaceans, such as *C. borealis*.

Increased atmospheric carbon dioxide is causing rises in both the temperature (Buchel et al., 1999; Macfarling et al., 2006) and dissolved carbon dioxide concentration of the world's oceans (Canadell et al., 2007; Knorr, 2009). If current trends continue, estimates reveal that these changes will reduce the average ocean pH from 8.1 to 7.6 in the next century (Wittman and Pörtner, 2013). The effects of ocean acidification are noticeably disrupting marine ecosystems (Kelly and Hofmann, 2013; Webb et al., 2016). In the lobster, *Homarus americanus*, prolonged thermal stress results in pH acidosis, hyperchloremia, and hyperproteinemia (Dove et al., 2005) and has been linked to mortality (Pearce and Balcom, 2005). Further, shifts in hemolymph pH *in vitro* alter the frequency and strength of the lobster cardiac rhythm (Qadri et al., 2007).

In several marine invertebrates including *H. americanus* and the crab, *Carcinus maenas*, hemolymph pH varies inversely with temperature following the rules of constant relative alkalinity (Dove et al., 2005; Howell et al., 1973; Qadri et al., 2007; Truchot, 1973, 1986; Vogt and Regehr, 2001). In other words, as temperature increases,

hemolymph acidifies by approximately -0.016 pH/°C to maintain a constant ratio of pH to pOH through a process of bicarbonate buffering. Maintenance of this ratio in extra- and intracellular fluids is thought to be important for stabilizing macromolecular structure and function (Reeves, 1972, 1977; Somero, 1981; Truchot, 2003). Like hemolymph, intracellular pH generally decreases as temperature rises, but has been shown to change at varying rates in different tissues in the crab, *Callinectes sapidus* (Vogt and Regehr, 2001). Active mechanisms for the maintenance of intracellular pH have been suggested in the crab, *Cancer pagurus* (Golowasch and Deitmer, 1993).

Both temperature and pH alter the biophysical parameters governing the activity of ion channels and pumps in excitable membranes. Studies on the biophysical effects of pH on ion channels revealed attenuation of sodium, calcium, and potassium currents under acidic extracellular conditions (Doering and McRory, 2007; Hille, 1968; Mozhaev et al., 1970; Tombaugh and Somjen, 1996; Wanke et al., 1979; Zhou and Jones, 1996). In the frog myelinated nerve, changing extracellular saline from pH 7 to pH 5 reduces sodium currents by up to 60% in a membrane potential-dependent manner (Woodhull, 1973) which may be mediated by increased sodium channel inactivation (Courtney, 1979). In rat CA1 neurons, moderate pH shifts from 7.4 to 6.4 reversibly depressed and shifted the voltage dependence of sodium (15% attenuation; +3 mV shift) and calcium currents (60% attenuation; +8 mV shift). Further, this acidosis was sufficient to shift potassium current inactivation to more depolarized voltages (+10 mV) while moderate alkalosis up to pH 8.0 had the opposite effect (Tombaugh and Somjen, 1996). This reversible gating of sodium, calcium, and potassium channels may result from protonation of an acidic group with pK_a between 5.2 and 7.1 (Tombaugh and Somjen, 1996). Decreases in glutamatergic synaptic function (Billups and Atwell, 1996; Bloch et

al., 2001; Sinning et al., 2011) and increases in GABAergic synaptic function (Sinning and Hübner, 2013) in response to decreases in pH have also been shown.

Although the biophysical, ethological, and environmental implications of changing pH have been well studied, less is known about the effect of pH changes on neuronal circuits in marine invertebrates. Here, we study the effects of acute changes in extracellular pH on two well characterized neuronal circuits, the stomatogastric (STG) and cardiac (CG) ganglia, of the crab, *C. borealis*. These central pattern generators (CPGs) drive the coordinated and rhythmic muscle movements of the crab's stomach and heart, respectively. Although these CPGs are driven by numerically small neuronal circuits, their dynamics involve complex interactions between many intrinsic and synaptic currents.

Previous studies have shown that the pyloric rhythm of the STG and cardiac rhythm of the CG are remarkably robust to short- and long-term changes in temperature in both *in vivo* and *ex vivo* preparations (Kushinsky et al., 2018; Marder et al., 2015; Soofi et al., 2014; Tang et al., 2010; Tang et al., 2012). Despite similarly robust activity under moderate perturbation, these experiments have revealed animal-to-animal variability in network activity at extreme temperatures (Haddad and Marder, 2018; Tang et al., 2010; Tang et al., 2012). In accordance with these findings, we reveal that both the pyloric and cardiac rhythms are remarkably robust to acute pH changes from 5.5 to 10.4. This is surprising given the sensitivity of many ion channels to pH in these ranges and suggests that networks can be more robust to pH changes than expected.

Results

Two neuronal networks were studied in this paper. The stomatogastric ganglion (STG) of the crab, *Cancer borealis*, contains the neurons that generate two stomach rhythms, the fast pyloric rhythm and the slower gastric mill rhythm. The pyloric rhythm is driven by a three-neuron pacemaker kernel – one Anterior Burster (AB) and two Pyloric Dilator (PD) neurons. The Lateral Pyloric (LP) and Pyloric (PY) neurons fire out of phase with the PD neurons because they are rhythmically inhibited by the PD/AB group (Marder and Bucher, 2007). The cardiac ganglion (CG) generates the rhythm responsible for heart contraction, and consists of four pacemaker Small Cell (SC) neurons that drive five motor Large Cell (LC) neurons (Cooke, 2002).

A schematic diagram of the stomatogastric nervous system preparation is found in Figure 1A. Intracellular recordings were made from the somata of the desheathed STG and examples of the LP and PD neuron waveforms are shown. Extracellular recordings from the motor nerves are indicated by the gray circles. An example of the triphasic activity of the LP, PD, and PY neurons is seen in the inset trace next to the lateral ventricular nerve (*lvn*). The connectivity diagram of the major neuron classes of the triphasic pyloric rhythm is given in Figure 1B.

A schematic diagram of the crab cardiac ganglion preparation shows an example of one burst of SC and LC activity recorded from the trunk (Figure 1C). Figure 1D shows the connectivity diagram of the cardiac ganglion.

The Pyloric rhythm is surprisingly robust to extreme changes in pH

To characterize the response of the pyloric rhythm to acute changes in pH, superfused saline was exchanged every 15 minutes in steps of approximately pH 0.5

94 from a control pH of 7.8 to an extreme pH of either 5.5 or 10.4. Following the first acid
95 or base step protocol, preparations were allowed to recover for a minimum of 30
96 minutes at control pH until the frequency of the pyloric rhythm approached that of
97 controls. Preparations were then subjected to a step protocol in the opposite direction
98 followed by a second recovery period. Acid- or base-first protocols were
99 counterbalanced.

100 Recordings and analysis from an example STG experiment with an acid-first
101 protocol are shown in Figure 2. Each box contains simultaneous intracellular recordings
102 of the PD and LP neurons and extracellular recordings of the *lvn* during the last minute
103 at each pH step (Figure 2A). STG #1 demonstrated a normal triphasic rhythm in control
104 saline at pH 7.8 (Figure 2A; top left). As the preparation was subjected to more acidic
105 saline, the rhythm remained triphasic until the most acidic pH, 5.5. Control activity was
106 recovered when the preparation was once again placed in control saline (Figure 2A; top
107 right). The bottom row shows the same preparation in basic conditions where it
108 remained triphasic, although with fewer spikes per burst and lower amplitude slow
109 waves at pH 10.4. Again, the preparation recovered a canonical triphasic rhythm in
110 control saline as seen in the bottom right.

111 Measures of the pyloric rhythm burst frequency, PD spikes per burst, and PD
112 duty cycle (the fraction of the pyloric rhythm's period during which the PD neurons
113 were active) were calculated for a period of steady state activity (the last eight minutes of
114 each 15-minute pH step). Violin plots reveal the distribution of these measures for STG
115 #1 at each pH (Figure 2B-D). The pyloric burst frequency of STG #1 increased in acid
116 and decreased in base (Figure 2B). The number of PD spikes per burst decreased at pH

117 5.5 (Figure 2C). The duty cycle of the PD neurons in STG #1 decreased slightly in both
118 acid and base (Figure 2D).

119 While some preparations maintained surprisingly robust pyloric rhythms from
120 pH 5.5 to 10.4, others exhibited disrupted patterns of activity at the most extreme pH
121 conditions. The activity of two additional STG preparations across the range of pH
122 tested is shown in Figure 3A. Both preparations displayed robust activity across a nearly
123 three-fold range of hydrogen ion concentration but became weakly active or silent at pH
124 5.5. At pH 10.4, STG #2 was slow and weakly triphasic while STG #3 retained a strong
125 triphasic rhythm. These examples highlight both the animal-to-animal variability of the
126 pyloric rhythm at control conditions and the variable effects of extreme acidosis or
127 alkylosis on this network.

128 To characterize these effects across all preparations, we defined five states of
129 activity: 1) 'normal triphasic' rhythm containing PD, LP, and PY with a minimum of
130 three spikes per burst for each unit; 2) 'weak triphasic' rhythm retaining all 3 units with
131 some units spiking only once or twice per cycle; 3) 'intermittent triphasic' rhythm
132 describing rhythmic activity with only some units active; 4) 'all silent'; and 5) 'atypical
133 activity' or activity that could not be categorized under the first four definitions (Figure
134 3B). Preparations were categorized systematically according to the criteria outlined in
135 Materials and Methods. The mean fraction of time that all preparations spent in these
136 five states at steady state was analyzed (Figure 3C). Both acid and base significantly
137 decreased the fraction of time that preparations were rhythmic, a combined metric of
138 states 1 (normal triphasic) and 2 (weak triphasic) (Figure 3–figure supplement 1).
139 Preparations were significantly less triphasically rhythmic at pH 5.5 and pH 10.4
140 compared to control pH 7.8.

To describe these effects quantitatively, measures of the pyloric rhythm frequency, the number of PD spikes per burst, and PD duty cycle were calculated. Violin plots give pooled distributions for each pH across all preparations (Figure 3D-F). Mean pyloric burst frequency was relatively invariant across pH values in the presence of acid, but varied significantly across base steps (Figure 3D). Pyloric burst frequency at pH 9.3 and 10.4 was significantly slower than that at control. Both acid and base significantly affected the mean number of PD spikes per burst (Figure 3E). The number of spikes per burst was significantly reduced at pH 5.5. Additionally, there was a significant effect of acid and base on the mean PD duty cycle (Figure 3F). Paired samples t-tests revealed a slight increase in mean PD duty cycle from control pH 7.8 to pH 6.1.

The pooled distributions for these three measures were highly variable for all pH conditions reflecting the animal-to-animal variability in the pyloric rhythm. We plotted the distributions for all 15 STG preparations at control pH 7.8 and found similarly variable activity at baseline conditions (Figure 3–figure supplement 2).

Isolated pyloric neurons are sensitive to extreme pH

To determine how the intrinsic properties of isolated neurons respond to pH, we analyzed several characteristics of the intracellular recordings from the PD and LP neurons (Figure 4). We isolated the neurons from most of their pyloric network synaptic inputs by blocking the glutamatergic inhibitory synapses with 10^{-5} M picrotoxin (PTX) (Marder and Eisen, 1984)(Figure 1B). We analyzed mean resting membrane potential (mV), spike amplitude (mV), and burst or spiking frequencies (Hz) for both cells in the presence of PTX as a function of pH. The waveforms of the PD and LP neurons from an example preparation are shown prior to PTX superfusion (Figure 4A; leftmost traces).

Note the large LP-evoked inhibitory post-synaptic potentials (IPSPs) in the trough of the PD neuron waveform and the large amplitude inhibition of the LP caused by activity of the PD, AB, and PY neurons. Following application of PTX at control pH 7.8 (Figure 4A; center traces), the PD neuron was still bursting but the LP-evoked IPSPs were entirely blocked. Most of the inhibitory inputs to the LP neuron were blocked, leaving only the cholinergic inhibition contributed by the PD neurons. At pH 6.7, the PD neuron of this preparation lost most of its slow wave activity. It then became silent and depolarized in pH 5.5 saline. At pH 8.8, the PD burst was largely intact, and at pH 10.4, the neuron showed single spike bursts. The LP neuron fired tonically from pH 6.7 to 10.4, again showing loss of activity at pH 5.5 similar to PD.

Violin plots show pooled values for the most hyperpolarized levels (minimum voltages) of the membrane potential for PD and LP neurons (Figure 4B,C). For moderate shifts in pH, the membrane potential was fairly stable. At extreme acid, the mean PD neuron membrane potential depolarized significantly, while the mean LP neuron membrane potential remained relatively constant (Figure 4–figure supplement 1). In contrast, the PD neuron's membrane potential in basic saline was relatively constant, even at extreme base, but the LP neuron's membrane potential significantly hyperpolarized. The depolarization of PD at pH 5.5 and 6.1 and the hyperpolarization of LP at pH 8.8, 9.3, 9.8, and 10.4 were significantly different from control saline.

Additionally, there was a slight effect of pH on mean spike amplitude at the most extreme pH conditions for both the LP and PD neurons (Figure 4D,E). Acid significantly affected both PD and LP neuron spike amplitude while alkylosis had an effect on the LP, but not the PD neurons (Figure 4–figure supplement 1). At pH 5.5 spike amplitude was

188 significantly attenuated for both LP and PD. Additionally, LP spike amplitude was
189 significantly decreased at pH 6.1 while PD was only moderately affected.
190 There was a significant effect of both acidic and basic saline on mean PD burst
191 frequency and LP firing rate (Figure 4F,G; Figure 4–figure supplement 1). Mean PD
192 burst frequency was significantly decreased at pH 5.5. The LP firing rate was
193 significantly reduced in pH 5.5, 6.1, 8.3, 9.3, 9.8, and 10.4 compared to control pH 7.8.
194
195 ***Rhythmic gastric-like activity was elicited upon exposure to and recovery***
196 ***from extreme acid and base***
197 The STG contains a second slower central pattern generating circuit known as the
198 gastric mill rhythm (Marder and Bucher, 2007). Unlike the pyloric rhythm which
199 contains a pacemaker kernel, the gastric rhythm is controlled by the reciprocal
200 alternation of activity driven by descending neuromodulatory inputs (Marder and
201 Bucher, 2007; Nusbaum et al., 2017). The principal neurons involved in the gastric mill
202 rhythm are the Lateral Gastric (LG), Medial Gastric (MG), Lateral Posterior Gastric
203 (LPG), Gastric Mill (GM), Dorsal Gastric (DG), and Interneuron 1 (Int1) neurons
204 (Mulloney and Selverston, 1974a, b).
205 The gastric mill rhythm is often silent in dissected STG preparations and requires
206 stimulation of descending and/or sensory neurons to elicit activity (Blitz et al., 1999).
207 Interestingly, in 10 of 15 preparations a gastric-like rhythm appeared at pH 8.8 or
208 above, and 4 of 15 showed this type of activity in acid at or below pH 6.1. Further, a
209 strong gastric-like rhythm was elicited upon recovery from extreme acid in 5 of 15
210 preparations and from extreme base in 7 of 15. Preparations in which gastric rhythms

were seen in one of these conditions were likely to display gastric-like activity in the other conditions.

An example preparation in control pH 7.8 saline is shown as it recovers activity after exposure to pH 5.5 saline (Figure 5). Intracellular recordings from the LP and PD neurons and extracellular recordings from five nerves – lateral ventricular (*lvn*), medial ventricular (*mvn*), dorsal gastric (*dgn*), lateral gastric (*lgn*), and inferior oesophageal (*ion*) – are shown. In addition to axons of the LP, PD, and PY neurons, the *lvn* contains the LG axon. The *mvn* contains axons from two neurons, the Inferior Cardiac (IC) and the Ventricular Dilator (VD). Inhibition of IC and VD was coincident with LG bursting. The *dgn* shows GM and DG activity and the *lgn* contains LG activity. Recordings from the *ion* reveal Modulatory Commissural Neuron 1 (MCN1) activity. One period of the gastric mill rhythm can be defined by the time from the onset of one LG burst to the next.

Over the 20 minutes shown, there was a clear increase in both gastric and pyloric activity with the LP and PD neurons becoming rhythmic and the emergence of strong rhythmic activity of the MCN1, LG, DG, and GM neurons (Figure 5A). At the beginning of this recovery period, both the PD and LP neurons were silent, reflecting loss of activity in pH 5.5 (Figure 5B). Strong LG neuron bursts were timed with hyperpolarizations of the LP neuron. This is consistent with previous findings that the neurons driving the gastric mill rhythm synapse onto the pyloric network and that gastric mill activity correlates with slowing of the pyloric rhythm (Bucher et al., 2007). A few minutes later, the LP and PD neurons started to recover rhythmic slow waves (Figure 5C). The LP and the second PD neuron – seen here on the *lvn* recording – were bursting. Both neurons became silent due to a strong inhibitory input coinciding with

strong LG and MCN1 activity. Shortly thereafter, the LP and PD neurons were firing rhythmically (Figure 5D). Depolarizing inhibition resulted in tonic firing of LP and no activity on the intracellular recording of PD. Finally, the LP and PD neurons were bursting (Figure 5E). Inhibitory input coincident with LG and MCN1 activity resulted in depolarization of the PD and LP neurons and an increased duty cycle of LP bursting.

The rhythmic gastric-like activity seen here is similar to gastric mill rhythms elicited upon stimulation of the Ventral Cardiac Neurons (VCNs) (Beenhakker et al., 2007; Saideman et al., 2007; White and Nusbaum, 2011). Studies have shown that stimulation of the VCNs triggers activation of MCN1 and Commissural Projection Neuron 2 (CPN2) in the commissural ganglia (CoGs). This MCN1/CPN2 gastric mill rhythm drives the alternation of activity of the protractor motor neurons – LG, GM, MG, and IC – and the retractor neurons – DG, Int 1, and VD. We see similar activity here with strong MCN1 bursts on the *ion* corresponding to strong LG and GM bursts on the *lgn* and *dgn*, respectively, in alternation with DG bursts on the *dgn*.

The cardiac rhythm is robust to acute changes in pH

To characterize the response of the cardiac rhythm to pH, we bath superfused cardiac ganglion preparations with saline between pH 5.5 and pH 10.4 using the same protocol described above for stomatogastric ganglion preparations. Example extracellular recordings are shown from the cardiac ganglia of two animals during the last minute of each pH step (Figure 6A). As shown in the top row of CG #1, the ganglion started in control saline at pH 7.8 and demonstrated a normal rhythm of Small and Large Cells bursting together. As the preparation was subjected to both acidic and basic saline, the rhythm remained. In contrast, the cardiac rhythm in CG #2 became less

rhythmic in pH 5.5 and in pH 9.8 and above. A normal bursting rhythm recovered after superfusion of control saline as seen in the bottom right.

Measures of cardiac ganglion rhythm frequency, LC spikes per burst, and LC duty cycle were calculated for CG #1. Violin plots reveal the distribution of these measures at each pH (Figure 6B-D). The cardiac frequency of CG #1 decreased in acid and increased in base (Figure 6B). Further, the number of LC spikes per burst increased in acid (Figure 6C) while the LC duty cycle for CG #1 decreased slightly in acid and base (Figure 6D). Similar to STG #1, CG #1 retained robust activity throughout the entire range of pH tested.

To characterize these effects, we defined four states of activity: 1) 'SC and LC bursting' rhythm containing both units with a minimum of one LC spike per SC burst; 2) 'SC bursting only' rhythm containing only SC bursts with no or inconsistent LC spiking; 3) 'all silent'; and 4) 'atypical activity' that could not be categorized under the first three definitions (Figure 7A). The mean fraction of time that all preparations spent in these states is plotted (Figure 7B). The mean fraction of time that preparations were rhythmic (state 1 – SC and LC bursting) was significant affected by both acid and base (Figure 7–figure supplement 1). Rhythmic activity was significantly decreased at pH 5.5, pH 9.3, pH 9.8, and pH 10.4 compared to control pH 7.8.

To describe these effects quantitatively, measures of rhythm frequency, the number of LC spikes per burst, and LC duty cycle were calculated and their distributions are displayed in violin plots (Figure 7C-E). Cardiac rhythm frequency declined in both acidic and basic saline (Figure 7C; Figure 7–figure supplement 1). At pH 10.4, the cardiac rhythm was significantly slower. The mean number of LC spikes per burst was significantly affected in both acid and base (Figure 7D). The number of LC spikes per

283 burst was significantly increased at pH 5.5 and pH 6.1 and decreased at pH 9.8 and pH
284 10.4. There was a significant effect of base but not acid on mean LC duty cycle (Figure
285 7E).

286 Similar to the STG, we observed a large spread in pooled measures across all pH
287 conditions, reflecting the animal-to-animal variability in these networks. We plotted the
288 distributions for all CG preparations at baseline and noted highly variable cardiac
289 rhythm activity independent of the pH perturbation (Figure 7–figure supplement 2).
290

291 ***The cardiac and pyloric rhythms are differentially sensitive to pH***

292 To compare the effect of pH on the cardiac and pyloric rhythms, the distributions
293 of the fraction of time that each preparation retained a normal rhythm were compared
294 (Figure 8A). A normal rhythm was defined as a triphasic rhythm (a combined metric of
295 states 1 and 2) and Small Cells and Large Cells bursting together (state 1) for the pyloric
296 and cardiac rhythms, respectively. A comparison between the rhythmicity of these two
297 ganglia across pH reveals similar distributions with maxima around control pH 7.8 and
298 minima at extreme pH values. Interestingly, these distributions are asymmetrical, as the
299 CG was more sensitive to extreme base whereas the STG was more sensitive to extreme
300 acid. There were significant main effects of pH and ganglion as well as an interaction
301 between pH and ganglion on rhythmicity in both acidic and basic solutions (Figure 8–
302 figure supplement 1). The pyloric rhythm was significantly less rhythmic at pH 5.5, but
303 significantly more rhythmic at 9.3 and 9.8 compared to the cardiac rhythm.

304 To understand better the amount of animal-to-animal variability in these two
305 rhythms, the activity of individual preparations was plotted in control pH 7.8, extreme
306 acid pH 5.5, and extreme base pH 10.4 (Figure 8B). Each box represents an individual

307 preparation and its color saturation corresponds to the fraction of time with a normal
308 rhythm. All preparations were rhythmically bursting at control pH – indicated by darkly
309 colored boxes – and became less rhythmic – lighter colored – in the presence of extreme
310 acid. However, 14 of 15 STG preparations ceased firing after 15 minutes of exposure to
311 pH 5.5. In contrast, only 6 of 15 CG preparations showed reductions in rhythmic activity
312 at pH 5.5. Three of the 15 CG preparations maintained a normal rhythm in every pH
313 condition. Interestingly, STG preparations that showed decrements in activity during
314 basic conditions were extremely susceptible to reductions in activity during extreme
315 acid. The opposite is true in CG preparations suggesting that activity in base is a better
316 predictor of acid activity in the STG and vice versa in the CG. This finding also suggests
317 that some preparations were more susceptible to the effects of pH than others.

Discussion

Circuit dynamics depend on the properties of the constituent neurons and their synaptic connections. Likewise, the intrinsic excitability of an individual neuron depends on the number and properties of its voltage- and time-dependent channels. Given that the physiological properties of ion channels are sensitive to pH (Anwar et al., 2017; Bayliss et al., 2015; Catterall, 2000; Cens et al., 2011; Cook et al., 1984; Doering and McRory, 2007; Guarina et al., 2017; Harms et al., 2017; Hille, 1968; Mahapatra et al., 2011; Marcanoti et al., 2010; Tombaugh and Somjen, 1996; Vilin et al., 2012; Zhou et al., 2018), one might imagine that a neuronal circuit might be as sensitive to changes in pH as its most sensitive ion channels. Therefore, it is surprising that both the pyloric rhythm of the STG and the cardiac ganglion rhythm in the crab, *C. borealis*, are relatively insensitive to acute pH change from about pH 6.1 to pH 8.8 while the individual functions of many ion channels are known to be considerably altered within this pH range.

One possibility is that crustacean ion channels are more robust to pH change than those that have been commonly studied. In most vertebrate animals, pH is carefully regulated. Slight acidosis or alkalosis can have deleterious effects on many aspects of vertebrate physiology (Chesler, 2003), which may be partially a consequence of the relative sensitivity of many vertebrate ion channels and synapses to pH. Unfortunately, little is known about the pH sensitivity of crustacean ion channels, but it would be surprising if it differed drastically from that seen in other animals as there is considerable homology across phylogeny in channel structure and function. However, it remains possible that modest evolutionary changes in channel structure occurred to allow endothermic animals to function in high temperature and low pH conditions.

342 A possible explanation for this circuit robustness may arise if there are
343 compensatory and/or correlated changes in the effects of pH across the population of
344 channels in these networks. Therefore, one prediction of the relative pH insensitivity of
345 these networks is that numerous pH sensitive changes occur across the population of
346 ion channels, but that these circuits have evolved sets of correlated ion channels that
347 compensate for these changes (O'Leary and Marder, 2016; O'Leary et al., 2013; O'Leary
348 et al., 2014; Temporal et al., 2012; Temporal et al., 2014; Tobin et al., 2009).
349 In addition to the relative pH insensitivity of these circuits, we were surprised
350 that the cardiac and pyloric rhythms of *C. borealis* are differentially sensitive to acid and
351 base. This was unexpected as many of the same ion channels are found in the two
352 ganglia (Northcutt et al., 2016; Ransdell et al., 2013a; Ransdell et al., 2013b; Schulz et
353 al., 2006; Schulz et al., 2007; Tobin et al., 2009). One possible explanation of this
354 intriguing finding could be due to differences in the burst generating mechanisms of the
355 two networks. The pyloric rhythm depends heavily on post-inhibitory rebound as a
356 timing mechanism (Harris-Warrick et al., 1995a; Harris-Warrick et al., 1995b; Hartline
357 and Gassie, 1979) while the cardiac ganglion depends on strong excitatory drive from
358 the pacemaker neurons (Cooke, 1988). These excitatory and inhibitory synaptic
359 connections could be differentially sensitive to pH. Additionally, although both
360 networks are driven by bursting pacemaker neurons, the contribution of different ion
361 channels to the burst generating mechanism may be sufficiently different in the two
362 cases such that the pacemakers themselves respond differently to high and low pH.
363 We also found that the membrane potential of the isolated pyloric neurons, LP
364 and PD, varied differentially with changing extracellular pH. Isolated LP neurons fired
365 tonically and hyperpolarized in extreme base while isolated PD neurons depolarized in

366 acid. In intact preparations, we observed depolarization in acid for both neurons,
367 suggesting an important role of synaptic input in regulating network activity across pH.
368 Together, these results illustrate the potential difficulty in generalizing the effects of
369 environmental perturbation across neurons and circuits, even within the same animal.

370 Additionally, we found that under most control conditions, the gastric mill
371 rhythm was silent as is typically observed in STG preparations. Unexpectedly, gastric
372 mill rhythms were frequently activated upon exposure to or recovery from extreme pH.
373 It is possible that either sensory or modulatory axons were activated by the pH changes,
374 and it is feasible that sensory and/or modulatory neurons might be part of a response to
375 altered pH.

376 In this study, we examined the effects of manipulating extracellular pH. However,
377 the extent to which intracellular pH was affected and its contribution to changes in
378 activity remain unclear. We observed that neurons penetrated with intracellular
379 recording electrodes exhibited more labile activity in response to changing pH. This may
380 indicate that changes in intracellular pH would be more deleterious than what occurs in
381 response to changes in extracellular pH alone. Golowasch and Deitmer (1993) revealed
382 that extracellular pH in the STG of the crab, *Cancer pagurus*, was reliably around 0.1
383 pH more alkaline than bath pH while intracellular pH was 0.3 to 0.4 pH more acidic.
384 Further, moderate shifts in bath pH – from pH 7.4 to 7.0 or 7.8 – resulted in negligible
385 changes in pyloric frequency and slow and low amplitude shifts in extracellular pH while
386 NH_4Cl induced acidosis resulted in recoverable alkylosis of both the intracellular and
387 extracellular space (Golowasch and Deitmer, 1993). These results suggest the restriction
388 of the free diffusion of protons through the ganglion and the existence of active Na^+-
389 dependent mechanisms to maintain more acidic intracellular and more alkaline

390 extracellular compartments. Golowasch and Deitmer (1993) hypothesize that glial cells
391 surrounding the neuronal processes in the neuropil of the STG may contain a Na^+/H^+
392 exchanger.

393 The ocean environment is both warming and acidifying at historic rates. *Cancer*
394 *borealis* maintains relatively robust pyloric and cardiac rhythms in the temperature
395 ranges it usually experiences, from 3°C to 25°C (Marder et al., 2015; Soofi et al., 2014;
396 Tang et al., 2010; Tang et al., 2012). Importantly, the effect of temperature on ocean pH
397 is relatively modest in comparison to the range of pH studied here. In *Carcinus meanus*,
398 exposure to artificial ocean acidification produced relatively small changes in
399 hemolymph pH (Maus et al., 2018). Therefore, unlike some ocean organisms that are
400 very sensitive to even small ocean pH changes, we predict that the neuronal circuits in
401 *C. borealis*, at least as an adult, will be largely insensitive to changes in ocean pH.
402 However, other physiological parameters, such as metabolic rates and hemolymph flow
403 may be more pH sensitive (Maus et al., 2018). Moreover, network performance may be
404 further attenuated when pH is coupled to increasing temperature and other
405 environmental insults.

406 Crab central pattern generating circuits are robust and adaptable to a large range
407 of temperatures (2009; Haddad and Marder, 2018; Rinberg et al., 2013; Tang et al.,
408 2010; Tang et al., 2012). Previous research revealed robust activity and increasing
409 frequency of the pyloric rhythm of the STG and cardiac rhythm of the CG in response to
410 increasing temperature in both *in vivo* and *ex vivo* preparations (Kushinsky et al., 2018;
411 Tang et al., 2010; Tang et al., 2012). Contrastingly, increasing pH reveals non-linear
412 effects on activity, which may suggest more complex mechanisms.

Finally, the data in this paper and in previous work on temperature reveal considerable animal-to-animal variability in response to extreme perturbations. Here, all preparations behaved predictably and reliably across more than a thousand-fold change in hydrogen ion concentration, an unexpectedly large range of robust performance. At more extreme pH, animal-to-animal variably became apparent, consistent with the responses of these circuits to extreme temperatures (Marder et al., 2015; Soofi et al., 2014; Tang et al., 2010; Tang et al., 2012). This animal-to-animal variability is almost certainly a consequence of the fact that similar network performance can arise from quite variable sets of underlying conductances (Goaillard et al., 2009; Grashow et al., 2009, 2010; Prinz et al., 2004). What remains to be seen is whether animals that are more robust to a given extreme perturbation are less robust to others and whether there are given sets of network parameters that confer robustness to many different perturbations.

426 ## Materials and Methods

427 ### *Animals*

428 From March 2016 to May 2018, adult male Jonah crabs (*Cancer borealis)*
429 weighing between 400 and 700 grams were obtained from Commercial Lobster (Boston,
430 MA). Before experimentation, all animals were housed in tanks with flowing artificial
431 seawater (Instant Ocean) between 10°C and 13°C on a 12-hour light/dark cycle without
432 food. Animals were kept in tanks for a maximum of two weeks. Animals were removed
433 from tanks and kept on ice for 30 minutes prior to dissection.

434

435 ### *Saline Solutions*

436 Control *C. borealis* physiological saline was composed of 440 mM NaCl, 11 mM
437 KCl, 13 mM $CaCl_2$, 26 mM $MgCl_2$, 11 mM Trizma base, and 5 mM Maleic acid. Additional
438 quantities of concentrated HCl and NaOH were added to achieve solutions with pH 5.5,
439 6.1, 6.7, 7.2, 7.8, 8.3, 8.8, 9.3, 9.8, and 10.4, at 11°C. Solution pH was measured using a
440 calibrated pH/ion meter (Mettler Toledo S220). For experiments with picrotoxin, 10^{-5} M
441 PTX was added to each of the pH solutions.

442

443 ### *Electrophysiology*

444 The stomatogastric and cardiac nervous systems were dissected out of the
445 animals and pinned out in a Sylgard (Dow Corning) coated plastic Petri dish containing
446 chilled saline (11°C). In all cases, we worked only with fully intact stomatogastric
447 nervous system preparations that included the commissural and esophageal ganglia and
448 their descending nerves. Only preparations containing healthy cardiac or pyloric
449 rhythms with no sign of damage from dissection were analyzed.

Vaseline wells were placed around motor nerves and extracellular recordings were obtained using stainless steel pin electrodes placed in the wells and amplified using a differential amplifier (A-M Systems Model 1700). Intracellular sharp-electrode recordings were obtained from cell bodies in the stomatogastric ganglion using a microelectrode amplifier (Molecular Devices Axoclamp 2B or 900A) with HS-2A-x1LU headstages holding 15-30 MΩ boroscilate microelectrodes with filaments (Sutter Instrument Co. BF150-86-10) pulled with a Flaming/Brown micropipette puller (Sutter Instrument Co. P-97). Microelectrodes were filled with a solution of 10 mM $MgCl_2$, 400 mM potassium gluconate, 10 mM HEPES, 15 mM Na_2SO_4, and 20 mM NaCl (Hooper et al., 2015).

Preparations were continuously superfused with physiological saline at 11°C. Superfusion was gravity fed at approximately nine mL/min. The temperature of the superfusing saline was controlled and recorded using a Peltier device (Warner Instruments CL-100). Instantaneous bath pH was recorded using a pH microelectrode placed adjacent to the ganglion (Thermo Scientific Orion 9810BN) combined with a preamplifier (Omega PHTX-21). Output from the pH microelectrode was converted from arbitrary voltage to pH using a temperature-compensated calibration.

Data Acquisition and Analysis

Data were acquired using a data acquisition board (Molecular Devices Digidata 1440A) and Clampex 10.5 software (Molecular Devices). Data were analyzed using Clampfit 10.5, Spike2 v 6.04 (Cambridge Electronic Design), and/or MATLAB 2017A (MathWorks). All code is available for download at github.com/jesshaley/haley_2018. Figures were prepared in Adobe Illustrator CC 2017.

For analyses of extracellular recordings of the *lvn* of the STG or the trunk of the CG, we analyzed the last eight minutes of each 15-minute pH step to ensure that preparations had reached a steady state.

Data were categorized into states by manual annotation. A transition from one state to another was noted when there was a sustained change in activity lasting a minimum of 10 seconds. In other words, if the rhythm transitioned from one state into another and maintained the new state of activity for at least 10 seconds, a transition was noted at the start of that new state. Rhythms rarely transitioned intermittently between two states (e.g. once a pyloric rhythm had transitioned from normal triphasic to weak triphasic, it rarely transitioned back to normal triphasic until after recovery in control pH). Further, rhythms generally transitioned in a stereotypical pattern. For STG preparations, the pyloric rhythm often transitioned from normal triphasic to weak triphasic to intermittent triphasic to all silent. For CG preparations, the cardiac rhythm usually transitioned from SC and LC bursting to SC bursting only to all silent. During recovery, these transition patterns were reversed. The mean fraction of time that the preparations remained in each state during the last eight minutes of recording at each pH step is plotted as stacked bar graphs.

Quantitative variables of frequency, number of spikes per burst, and duty cycle were measured using extracellular recordings. Spikes and bursts were first isolated in Spike2 by thresholding extracellular recordings. MATLAB was then used for further analysis. Instantaneous burst frequency was calculated by taking the inverse of the cycle's period, the time elapsed between the onset of one burst and the onset of the next. The number of spikes per burst of a given neuron reflects the number of spikes contributing to each burst. Duty cycle reflects the fraction derived by dividing the burst

498 duration – time elapsed between the first and last spike – by the burst period. Mean
499 values were computed for bins of 10 seconds such that for eight minutes of data, there
500 were 48 binned mean values for each preparation, condition, and measure. Violin plots
501 show distributions of these binned mean values pooled for all preparations. The body of
502 the violin is a rotated kernel density estimate (KDE) plot. The circles give the median of
503 the pooled data and the horizontal bars give the mean. The interquartile range (IQR) is
504 given by the box plot within each violin with the whiskers giving the 95 percent
505 confidence interval (CI).

506 For analyses of intracellular recordings of isolated LP and PD neurons, the last
507 minute of each pH step was analyzed in MATLAB. Minimum membrane potential was
508 first measured by finding the minimum voltage of the neuron between each burst.
509 Recordings were then low-pass filtered to remove spikes from the slow wave. Slow wave
510 amplitude was measured by subtracting the trough from the peak of the slow wave's
511 membrane potential. Spike amplitude was retrieved by subtracting the filtered slow
512 wave signal from the original recording and then measuring the amplitude from trough
513 to peak of each action potential. PD burst frequency was calculated by finding the
514 inverse of the time period between one slow wave trough to the next. LP firing rate was
515 determined by calculating the inverse of the inter-spike interval, the time between
516 spikes. Mean values were computed for bins of 10 seconds. Violin plots show
517 distributions of these binned mean values pooled for all preparations.

518

519 ***Statistics***

520 All statistics were performed using R (version 3.4.3). We performed statistical
521 testing of the effects of acid and base on measures of the cardiac and pyloric rhythms

using a Univariate Type III Repeated-Measures Analysis of Variance (ANOVA) from the car package. Separate tests were performed for acid and base step protocols. Post-hoc paired sample t-tests with Bonferroni correction were performed for each pH step against its respective control. To assess the differences between the effects of pH on the cardiac and pyloric rhythms, we performed a Two-Way Mixed-Measures ANOVA (Type III) for both acid and base step protocols using the car package. Post-hoc independent samples t-tests with Bonferroni correction were performed for each pH condition.

References

(2009). DFO. (Can Sci Advis Sec Sci Advi Rep).

Anwar, H., Li, X., Bucher, D., and Nadim, F. (2017). Functional roles of short-term synaptic plasticity with an emphasis on inhibition. Curr Opin Neurobiol 43, 71-78.

Bayliss, D.A., Barhanin, J., Gestrau, C., and Guyenet, P.G. (2015). The role of pH-sensitive TASK channels in central respiratory chemoreception. Pfluegers Arch/Eur J Physiol 467, 917-929.

Beenhakker, M.P., Kirby, M.S., and Nusbaum, M.P. (2007). Mechanosensory gating of proprioceptor input to modulatory projection neurons. J Neurosci 27, 14308-14316.

Billups, B., and Atwell, D. (1996). Modulation of non-vesicular glutamate release by pH. Nature 379, 171.

Blitz, D.M., Christie, A.E., Coleman, M.J., Norris, B.J., Marder, E., and Nusbaum, M.P. (1999). Different proctolin neurons elicit distinct motor patterns from a multifunctional neuronal network. J Neurosci 19, 5449-5463.

Bloch, W., Addicks, K., Hescheler, J., and Fleischmann, B.K. (2001). Nitric oxide synthase expression and function in embryonic and adult cardiomyocytes. Microsc Res Tech 55, 259-269.

Buchel, C., Coull, J.T., and Friston, K.J. (1999). The predictive value of changes in effective connectivity for human learning. Science 283, 1538-1541.

Bucher, D., Johnson, C.D., and Marder, E. (2007). Neuronal morphology and neuropil structure in the stomatogastric ganglion of the lobster, *Homarus americanus*. J Comp Neurol 501, 185-205.

Canadell, J.G., Le Quéré, C., Raupach, M.R., Field, C.B., Buitenhuis, E.T., Ciais, P., and Marland, G. (2007). Contributions to accelerating atmospheric CO_2 growth from economic activity, carbon intensity, and efficiency of natural sinks. Proc Natl Acad Sci USA 104, 18866-18870.

Catterall, W.A. (2000). From ionic currents to molecular mechanisms: the structure and function of voltage-gated sodium channels. Neuron 26, 13-25.

Cens, T., Rousset, M., and Charnet, P. (2011). Two sets of amino acids of the domain I of Cav2.3 Ca(2+) channels contribute to their high sensitivity to extracellular protons. Pfluegers Arch/Eur J Physiol 462, 303-314.

Chesler, M. (2003). Regulation and modulation of pH in the brain. Physiol Rev 83, 1183-1221.

Cook, D.L., Ikeuchi, M., and Fujimoto, W. (1984). Lowering of pH_i inhibits Ca^{2+}-activated K^+ channels in pancreatic B-cells. Nature 31, 269-271.

Cooke, I.M. (1988). Studies on the crustacean cardiac ganglion. Comp Biochem Physiol C 91, 205-218.

Cooke, I.M. (2002). Reliable, responsive pacemaking and pattern generation with minimal cell numbers: the crustacean cardiac ganglion. Biol Bull 202, 108-136.

Courtney, K.R. (1979). Extracellular pH selectively modulates recovery from sodium inactivation in frog myelinated nerve. Biophys J 28, 363-368.

Doering, C.J., and McRory, J.E. (2007). Effects of extracellular pH on neuronal calcium channel activation. Neuroscience 146, 1032-1043.

Donahue, M.J., Nichols, A., Santamaria, C.A., League-Pike, P.E., and Krediet, C.J. (2009). Predation risk, prey abundance, and the vertical distribution of three brachyuran crabs on Gulf of Maine shores. J Crust Biol 29, 523–531.

Dove, A.D.M., Allam, B., Powers, J.J., and Sokolowski, M.S. (2005). A Prolonged thermal stress experiment on the american lobster, *Homarus americanus*. J Shellfish Res 24, 761-765.

Goaillard, J.M., Taylor, A.L., Schulz, D.J., and Marder, E. (2009). Functional consequences of animal-to-animal variation in circuit parameters. Nat Neurosci 12, 1424-1430.

Golowasch, J., and Deitmer, J.W. (1993). pH regulation in the stomatogastric ganglion of the crab *Cancer pagurus*. J Comp Physiol, A 172, 573-581.

Grashow, R., Brookings, T., and Marder, E. (2009). Reliable neuromodulation from circuits with variable underlying structure. Proc Natl Acad Sci U S A 106, 11742-11746.

Grashow, R., Brookings, T., and Marder, E. (2010). Compensation for variable intrinsic neuronal excitability by circuit-synaptic interactions. J Neurosci 30, 9145-9156.

Guarina, L., Vandael, D.H., Carabelli, V., and Carbone, E. (2017). Low pH_o boosts burst firing and catecholamine release by blocking TASK-1 and BK channels while preserving Cav1 channels in mouse chromaffin cells. J Physiol 595, 2587-2609.

Haddad, S.A., and Marder, E. (2018). Circuit robustness to temperature perturbation is altered by neuromodulators. Neuron, in press.

Haeffner Jr, P.A. (1977). Aspects of the biology of the Jonah crab, *Cancer borealis* Stimpson, 1859 in the mid Atlantic Bight. J Nat Hist 11, 303–320.

Harms, E., Stoetzer, C., Stueber, T., O'Reilly, A.O., and Leffler, A. (2017). Investigation into the role of an extracellular loop in mediating proton-evoked inhibition of voltage-gated sodium channels. Neurosci Lett 661, 5-10.

Harris-Warrick, R.M., Coniglio, L.M., Barazangi, N., Guckenheimer, J., and Gueron, S. (1995a). Dopamine modulation of transient potassium current evokes phase shifts in a central pattern generator network. J Neurosci 15, 342-358.

Harris-Warrick, R.M., Coniglio, L.M., Levini, R.M., Gueron, S., and Guckenheimer, J. (1995b). Dopamine modulation of two subthreshold currents produces phase shifts in activity of an identified motoneuron. J Neurophysiol 74, 1404-1420.

Hartline, D.K., and Gassie, D.V., Jr. (1979). Pattern generation in the lobster (*Panulirus*) stomatogastric ganglion. I. Pyloric neuron kinetics and synaptic interactions. Biol Cybern 33, 209-222.

Hille, B. (1968). Charges and potentials at the nerve surface: divalent ions and pH. J Gen Physiol 51, 221-236.

Hooper, S.L., Thuma, J.B., Guschlbauer, C., Schmidt, J., and Buschges, A. (2015). Cell dialysis by sharp electrodes can cause nonphysiological changes in neuron properties. J Neurophysiol 114, 1255-1271.

Howell, B.J., Rahn, H., Goodfellow, D., and Herreid, C. (1973). Acid-base regulation and temperature in selected invertebrates as a function of temperature. Am Zool 13, 557-563.

Kelly, M.W., and Hofmann, G.E. (2013). Adaptation and the physiology of ocean acidification. Funct Ecol 27, 980-990.

Knorr, W. (2009). Is the airborne fraction of anthropogenic CO_2 emissions increasing? Geophys Res Lett 36.

Kushinsky, D., Morozova, E., and Marder, E. (2018). *In vivo* effects of temperature on the heart and pyloric rhythms in the crab, *Cancer borealis*. Submitted, BIORXIV/2018/249631.

Macfarling, M.C., Etheridge, D., Trudinger, C., Steele, P., Lagenfelds, R., Van Ommen, T., and Elkins, J. (2006). Law Dome CO_2, CH_4 and N_2O ice core records extended to 2000 years BP. Geophys Res Lett 33.

Mahapatra, S., Marcanoti, A., Vandael, D.H., Striessnig, J., and Carbone, E. (2011). Are Cav1.3 pacemaker channels in chromaffin cells? Possible bias from resting cell conditions and DHP blockers usage: Possible bias from resting cell conditions and DHP blocker usage. Channels 5, 219-224.

Marcanoti, A., Vandael, D.H., Mahapatra, S., Carabelli, V., Sinnegger-Brauns, M.J., Striessnig, J., and Carbone, E. (2010). Loss of Cav1.3 channels reveals the critical role of L-type and BK channel coupling in pacemaking mouse adrenal chromaffin cells. J Neurosci 30, 219-224.

Marder, E., and Bucher, D. (2007). Understanding circuit dynamics using the stomatogastric nervous system of lobsters and crabs. Annu Rev Physiol 69, 291-316.

Marder, E., and Eisen, J.S. (1984). Transmitter identification of pyloric neurons: electrically coupled neurons use different neurotransmitters. J Neurophysiol 51, 1345-1361.

Marder, E., Haddad, S.A., Goeritz, M.L., Rosenbaum, P., and Kispersky, T. (2015). How can motor systems retain performance over a wide temperature range? Lessons from the crustacean stomatogastric nervous system. J Comp Physiol, A 201, 851-856.

Maus, B., Book, C., and Pörtner, H.O. (2018). Water bicarbonate modulates the response of the shore crab Carcinus maenas to ocean acidification. J Comp Physiol, B 188, 749-764.

Mozhaev, G.A., Mozhaeva, G.N., and Naumov, A.P. (1970). Effect of calcium ions on the steady-state potassium conductivity of the Ranvier node membrane. Tsitologiia 12, 993-1001.

Mulloney, B., and Selverston, A.I. (1974a). Organization of the stomatogastric ganglion in the spiny lobster. I. Neurons driving the lateral teeth. J Comp Physiol 91, 1-32.

Mulloney, B., and Selverston, A.I. (1974b). Organization of the stomatogastric ganglion in the spiny lobster. III. Coordination of the two subsets of the gastric system. J Comp Physiol 91, 53-78.

Northcutt, A.J., Lett, K.M., Garcia, V.B., Diester, C.M., Lane, B.J., Marder, E., and Schulz, D.J. (2016). Deep sequencing of transcriptomes from the nervous systems of two decapod crustaceans to characterize genes important for neural circuit function and modulation. BMC Genomics 17, 868.

Nusbaum, M.P., Blitz, D.M., and Marder, E. (2017). Functional consequences of neuropeptide and small-molecule co-transmission. Nat Rev Neurosci 18, 389-403.

O'Leary, T., and Marder, E. (2016). Temperature-robust neural function from activity-dependent ion channel regulation. Current Biology 26, 2935-2941.

O'Leary, T., Williams, A.H., Caplan, J.S., and Marder, E. (2013). Correlations in ion channel expression emerge from homeostatic tuning rules. Proc Natl Acad Sci U S A 110, E2645-2654.

O'Leary, T., Williams, A.H., Franci, A., and Marder, E. (2014). Cell types, network homeostasis, and pathological compensation from a biologically plausible ion channel expression model. Neuron 82, 809-821.

Pearce, J., and Balcom, N. (2005). The 1999 Long Island Sound lobster mortality event: Findings of the comprehensive research initiative. J Shellfish Res 24, 133-139.

Prinz, A.A., Bucher, D., and Marder, E. (2004). Similar network activity from disparate circuit parameters. Nat Neurosci 7, 1345-1352.

Qadri, S.A., Camacho, J., Wang, H., Taylor, J.R., Grosell, M., and Worden, M.K. (2007). Temperature and acid–base balance in the American lobster *Homarus americanus*. J Exp Biol 210, 1245-1254.

Ransdell, J.L., Nair, S.S., and Schulz, D.J. (2013a). Neurons within the Same Network Independently Achieve Conserved Output by Differentially Balancing Variable Conductance Magnitudes. Journal of Neuroscience 33, 9950-9956.

Ransdell, J.L., Temporal, S., West, N.L., Leyrer, M.L., and Schulz, D.J. (2013b). Characterization of inward currents and channels underlying burst activity in motoneurons of crab cardiac ganglion. Journal of Neurophysiology 110, 42-54.

Reeves, R.B. (1972). An imidazole alphastat hypothesis for vertebrate acid-base regulation: Tissue carbon dioxide content and body temperature in bullfrogs. Respir Physiol 14, 219-236.

Reeves, R.B. (1977). The interaction of body temperature and acid-base balance in ectothermic vertebrates. Annu Rev Physiol 39, 559-586.

Rinberg, A., Taylor, A.L., and Marder, E. (2013). The effects of temperature on the stability of a neuronal oscillator. PLoS Comput Biol 9, e1002857.

Saideman, S.R., Blitz, D.M., and Nusbaum, M.P. (2007). Convergent motor patterns from divergent circuits. J Neurosci 27, 6664-6674.

Schulz, D.J., Goaillard, J.M., and Marder, E. (2006). Variable channel expression in identified single and electrically coupled neurons in different animals. Nat Neurosci 9, 356 - 362.

Schulz, D.J., Goaillard, J.M., and Marder, E.E. (2007). Quantitative expression profiling of identified neurons reveals cell-specific constraints on highly variable levels of gene expression. Proc Natl Acad Sci U S A 104, 13187-13191.

Sinning, A., and Hübner, C.A. (2013). Minireview: pH and synaptic transmission. FEBS Lett 587, 1923-1928.

Sinning, A., Liebmann, L., Kougioumtzes, A., Westermann, M., Bruehl, C., and Hübner, C.A. (2011). Synaptic glutamate release is modulated by the Na^+-driven Cl^-/HCO_3^- exchanger Slc4a8. J Neurosci 31, 7300-7311.

Somero, G.N. (1981). pH-temperature interactions on proteins: Principles of optimal pH and buffer system design. Mar Biol Lett 2, 163-178.

Soofi, W., Goeritz, M.L., Kispersky, T.J., Prinz, A.A., Marder, E., and Stein, W. (2014). Phase maintenance in a rhythmic motor pattern during temperature changes *in vivo*. J Neurophysiol 111, 2603-2613.

Stehlik, L.L., MacKenzie, C.L., and Morse, W.W. (1991). Distribution and abundance of four brachyuran crabs on the northwest Atlantic shelf. Fish Bull 89, 473–492.

Tang, L.S., Goeritz, M.L., Caplan, J.S., Taylor, A.L., Fisek, M., and Marder, E. (2010). Precise temperature compensation of phase in a rhythmic motor pattern. PLoS Biol 8, e1000469.

Tang, L.S., Taylor, A.L., Rinberg, A., and Marder, E. (2012). Robustness of a rhythmic circuit to short- and long-term temperature changes. J Neurosci 32, 10075-10085.

Temporal, S., Desai, M., Khorkova, O., Varghese, G., Dai, A., Schulz, D.J., and Golowasch, J. (2012). Neuromodulation independently determines correlated channel expression and conductance levels in motor neurons of the stomatogastric ganglion. J Neurophysiol 107, 718-727.

Temporal, S., Lett, K.M., and Schulz, D.J. (2014). Activity-dependent feedback regulates correlated ion channel mRNA levels in single identified motor neurons. Curr Biol 24, 1899-1904.

Tobin, A.E., Cruz-Bermudez, N.D., Marder, E., and Schulz, D.J. (2009). Correlations in ion channel mRNA in rhythmically active neurons. PLoS ONE 4, e6742.

Tombaugh, G.C., and Somjen, G.G. (1996). Effects of extracellular pH on voltage-gated Na^+, K^+ and Ca^{2+} currents in isolated rat CA1 neurons. J Physiol 493, 719-732.

Truchot, J.-P. (1973). Mechanisms of extracellular acid-base regulation as temperature changes in decapod crustaceans. Respir Physiol 33, 161-176.

Truchot, J.-P. (1986). Changes in the hemolymph acid-base state of the shore crab, *Carcinus maenas*, exposed to simulated tidepool conditions. Biol Bull 170, 506-518.

Truchot, J.-P. (2003). Temperature and acid-base regulation in the shore crab *Carcinus maenas* (L.). Respir Physiol 17, 11-20.

Vilin, Y.Y., Peters, C.H., and Ruben, P. (2012). Acidosis differentially modulates inactivation in $Na_v1.2$, $Na_v1.4$, and $Na_v1.5$ channels. Front Pharmacol 3, 109.

Vogt, K.E., and Regehr, W.G. (2001). Cholinergic modulation of excitatory synaptic transmission in the CA3 area of the hippocampus. J Neurosci 21, 75-83.

Wanke, E., Carbone, E., and Testa, P.L. (1979). K^+ conductance modified by a titratable group accessible to protons from the intracellular side of the squid axon membrane. Biophys J 26, 319-324.

Webb, S.J., Tu, J., Cory, E., Morgan, V., Sah, R., Deheyn, D.D., and Taylor, J.R. (2016). Stress physiology and weapon integrity of intertidal mantis shrimp under future ocean conditions. Sci Rep 6, 38637.

White, R.S., and Nusbaum, M.P. (2011). The same core rhythm generator underlies different rhythmic motor patterns. J Neurosci 31, 11484-11494.

Wittman, A.C., and Pörtner, H.O. (2013). Sensitivities of extant animal taxa to ocean acidification. Nat Clim Change 3, 995.

Woodhull, A.M. (1973). Ionic blockage of sodium channels in nerve. J Gen Physiol 61, 687-708.

Zhou, W., and Jones, S.W. (1996). The effects of external pH on calcium channel currents in bullfrog sympathetic neurons. Biophys J 70, 1326-1334.

Zhou, Y., Xia, X.-M., and Lingle, C.J. (2018). BK channel inhibition by strong extracellular acidification. eLife 7, e38060.

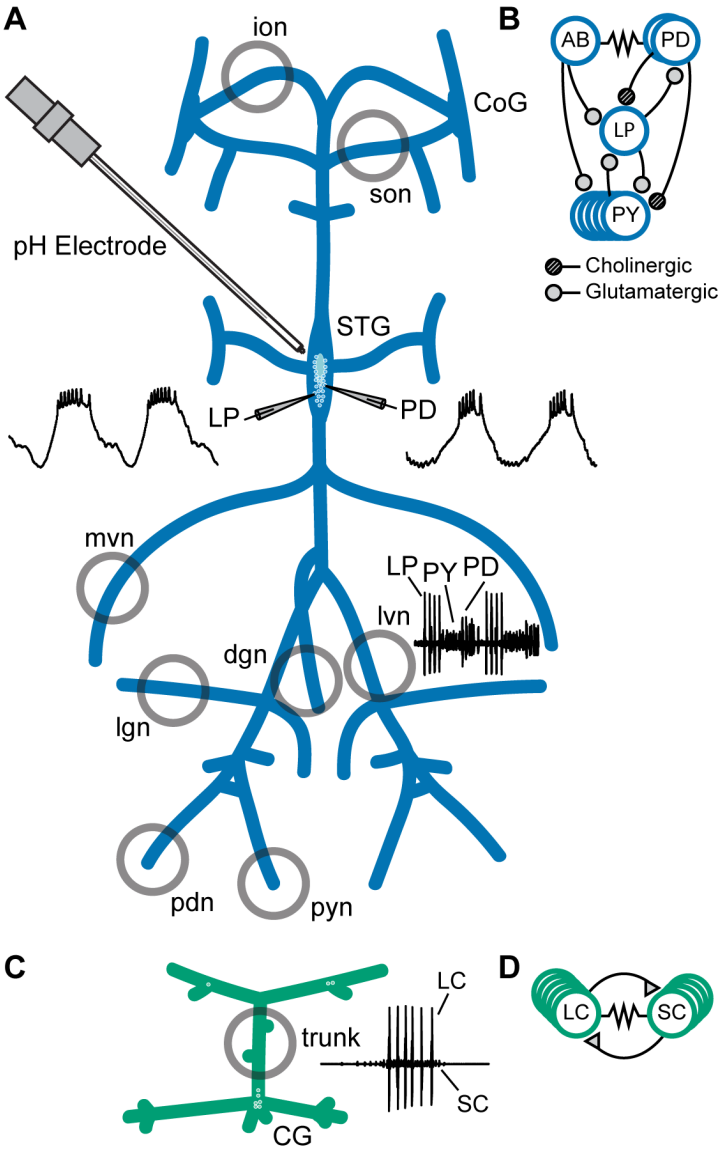

Figure 1. Preparations and circuit diagrams.
(A) Schematic of the stomatogastric nervous system preparation. Extracellular electrodes were placed in vaseline wells (gray circles) drawn around nerves of interest. An example extracellular nerve recording from the lateral ventricular nerve (*lvn*) shows two cycles of the triphasic pyloric rhythm containing spikes from the Lateral Pyloric (LP), Pyloric (PY), and Pyloric Dilator (PD) neurons. Example intracellular recordings from the LP and PD neurons are displayed. **(B)** Simplified diagram of the pyloric circuit. Filled circles represent inhibitory chemical synapses; resistor symbol represents electrical coupling. **(C)** Schematic of the cardiac ganglion preparation. Extracellular electrodes were placed in a well (gray circle) around the trunk of the preparation. An example extracellular recording shows one burst of the Small Cell (SC) and Large Cell (LC) neurons. **(D)** Diagram of the cardiac circuit. Filled triangles represent excitatory chemical synapses; the resistor symbol represents electrical coupling.

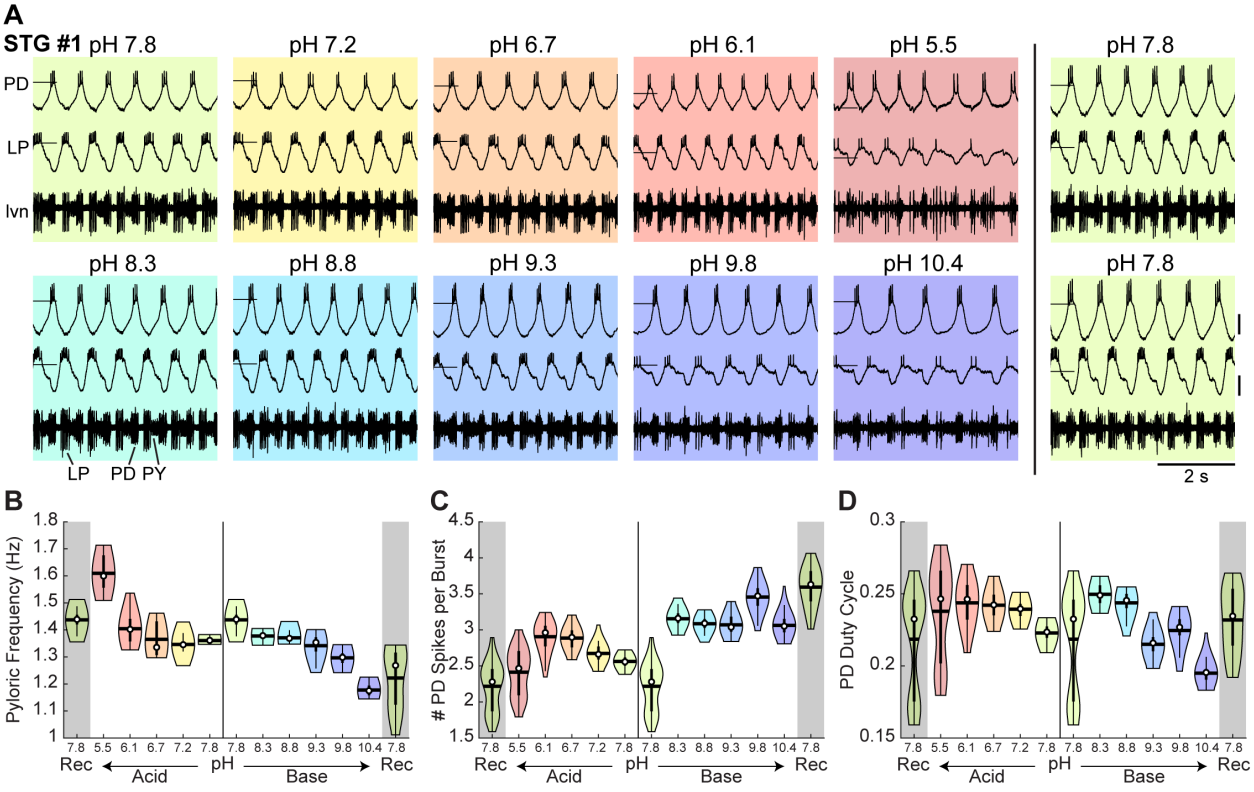

Figure 2. Robust pyloric rhythm activity across pH.
(A) Example recordings from a stomatogastric ganglion experiment with an acid-first protocol. Intracellular recordings of the PD and LP neurons and extracellular recordings of the *lvn* are shown. Each colored box displays five seconds of recordings taken from the last minute at each pH step. The experiment can be read left to right then top to bottom in chronological order. Horizontal lines indicate a reference membrane potential of -40 mV; vertical lines indicate a scale of 10 mV. **(B)** Pyloric frequency, **(C)** number of PD spikes per burst, and **(D)** PD duty cycle were calculated for the last eight minutes of each pH step. Violin plots show the KDE distribution, mean, median, IQR, and 95% CI for each measure across pH conditions. Recoveries from acid and base are displayed in the shaded gray regions on the far ends of each plot.

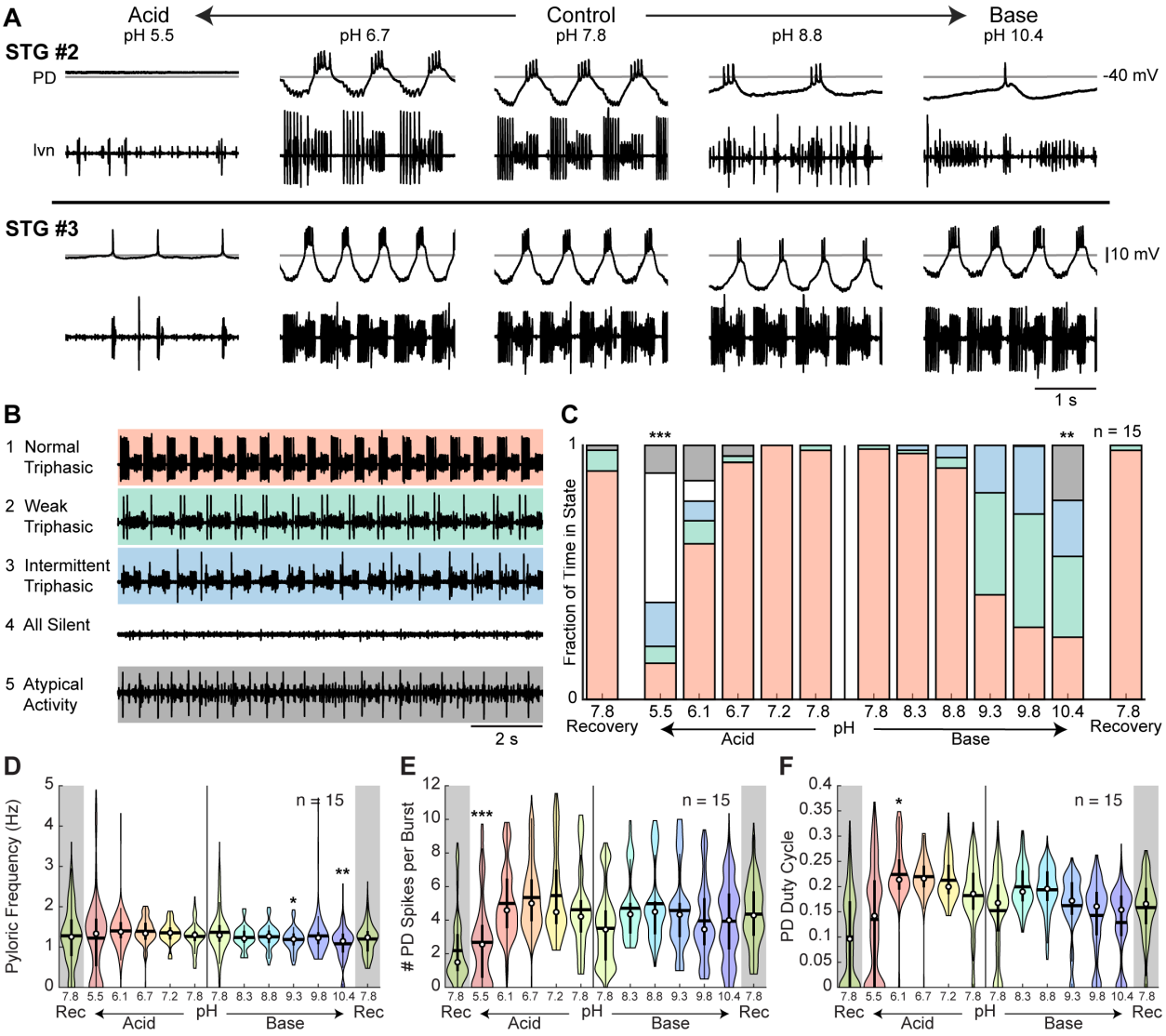

Figure 3. Variability of pyloric rhythm activity at extreme pH.
(A) Two additional stomatogastric ganglion experiments displaying three seconds of intracellular PD and extracellular *lvn* recordings. Horizontal lines indicate a reference membrane potential of -40 mV; vertical line indicates a scale of 10 mV. **(B)** Five states were defined to characterize pyloric rhythm activity. Examples of activity for each state are given. **(C)** Stacked bars give the mean fraction of time that all 15 preparations spent in each state. **(D)** Pyloric rhythm frequency, **(E)** number of PD spikes per burst, and **(F)** PD duty cycle were calculated and pooled across all STG preparations for each pH step. Violin plots show the KDE distribution, mean, median, IQR, and 95% CI for each measure across pH conditions. Recoveries from acid and base are displayed in the shaded gray regions on the far ends of each plot. Asterisks denote statistical significance revealed by paired samples t-tests with Bonferroni correction (*p<0.05; **p<0.01; ***p<0.001).

	One-Way Repeated Measures ANOVA	
Measure	**Acid**	**Base**
C - Time Rhythmic	F(4,56) = 33.466, p < 0.0001	F(5,70) = 8.188, p < 0.0001
D - Pyloric Freq	F(4,56) = 0.559, p = 0.6937	F(5,70) = 3.584, p = 0.0061
E - PD Spikes/Burst	F(4,56) = 16.774, p < 0.0001	F(5,70) = 3.443, p = 0.0077
F - PD Duty Cycle	F(4,56) = 10.671, p < 0.0001	F(5,70) = 6.231, p < 0.0001

	Paired Samples T-Tests with Bonferroni Correction			
Measure	**pH 5.5**	**pH 6.1**	**pH 6.7**	**pH 7.2**
C - Time Rhythmic	t(14) = 9.860, p < 0.0001	t(14) = 2.601, p = 0.0838	t(14) = 1.000, p = 1.3371	identical data
D - Pyloric Freq				
E - PD Spikes/Burst	t(14) = 5.696, p = 0.0002	t(14) = -1.197, p = 1.0054	t(14) = -2.121, p = 0.2089	t(14) = -1.871, p = 0.3295
F - PD Duty Cycle	t(14) = 2.257, p = 0.1621	t(14) = -3.040, p = 0.0353	t(14) = -2.828, p = 0.0536	t(14) = -2.853, p = 0.0511

	Paired Samples T-Tests with Bonferroni Correction				
Measure	**pH 8.3**	**pH 8.8**	**pH 9.3**	**pH 9.8**	**pH 10.4**
C - Time Rhythmic	t(14) = 1.000, p = 1.6714	t(14) = 1.000, p = 1.6714	t(14) = 2.014, p = 0.3181	t(14) = 2.296, p = 0.1883	t(14) = 3.953, p = 0.0072
D - Pyloric Freq	t(14) = 2.454, p = 0.1390	t(14) = 2.347, p = 0.1708	t(14) = 3.240, p = 0.0297	t(14) = 1.235, p = 1.1863	t(14) = 3.947, p = 0.0073
E - PD Spikes/Burst	t(14) = -2.609, p = 0.1030	t(14) = -2.947, p = 0.0530	t(14) = -2.104, p = 0.2698	t(14) = -0.853, p = 2.0408	t(14) = -0.652, p = 2.6240
F - PD Duty Cycle	t(14) = -2.108, p = 0.2678	t(14) = -2.034, p = 0.3066	t(14) = -0.463, p = 3.2535	t(14) = 0.470, p = 3.2287	t(14) = 1.156, p = 1.3344

Figure 3—figure supplement 1. Statistical analysis of the effects of pH on the pyloric rhythm.

The main effects of acid and base protocols on four measures of the activity of the pyloric rhythm were assessed. Univariate Type III Repeated-Measures Analysis of Variance (ANOVA) tests were performed separately for both acid and base step protocols. Post-hoc paired samples t-tests with Bonferroni correction were performed for each pH step against its respective control, the pH 7.8 condition immediately prior to the step protocol.

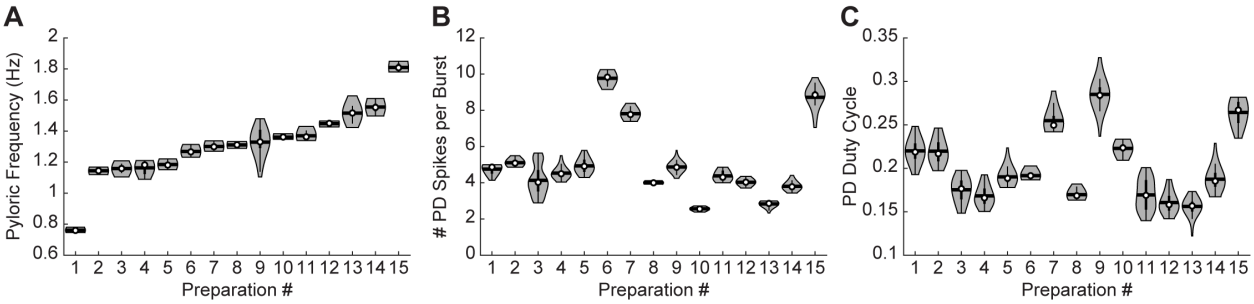

Figure 3—figure supplement 2. Variability of pyloric rhythm activity at control pH. **(A)** Pyloric rhythm frequency, **(B)** number of PD spikes per burst, and **(C)** PD duty cycle were calculated for each CG preparation for the last eight minutes in control pH 7.8. Violin plots show the KDE distribution, mean, median, IQR, and 95% CI for each measure across preparations. Preparations are consistent across plots and sorted in order of increasing frequency.

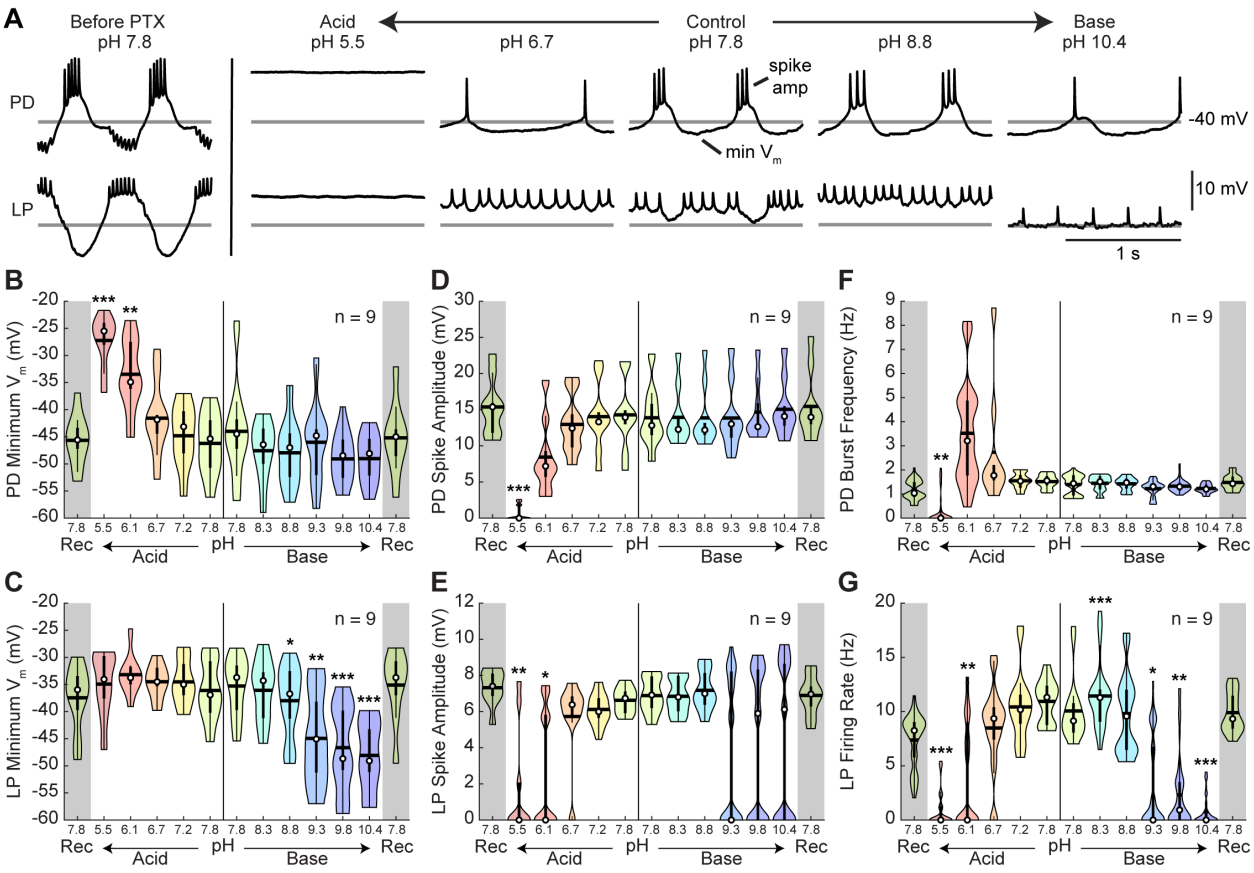

Figure 4. Intracellular characteristics of isolated pyloric neurons, PD and LP. Several characteristics of the PD and LP neurons in the presence of picrotoxin (PTX) were measured for the last minute of each pH condition. **(A)** Example intracellular recordings of PD and LP neurons prior to PTX application and in the presence of PTX across pH conditions. Horizontal lines indicate a reference membrane potential of -40 mV; the vertical line indicates a scale of 10 mV. **(B,C)** Minimum membrane potential and **(D,E)** spike amplitude are plotted for LP and PD as a function of pH. **(F)** PD burst frequency and **(G)** LP firing rate are also plotted at each pH. Violin plots show the KDE distribution, mean, median, IQR, and 95% CI for each measure across pH conditions. Recoveries from acid and base are displayed in the shaded gray regions on the far ends of each plot. Asterisks denote statistical significance revealed by paired samples t-tests with Bonferroni correction (*p<0.05; **p<0.01; ***p<0.001).

	One-Way Repeated Measures ANOVA	
Measure	**Acid**	**Base**
B - PD Min V_m	F(4,32) = 35.198, p < 0.0001	F(5,40) = 1.689, p = 0.1595
C - LP Min V_m	F(4,32) = 1.247, p = 0.3112	F(5,40) = 44.122, p < 0.0001
D - PD Spike Amp	F(4,32) = 30.004, p < 0.0001	F(5,40) = 1.235, p = 0.3109
E - LP Spike Amp	F(4,32) = 8.107, p = 0.0001	F(5,40) = 3.543, p = 0.0096
F - PD Burst Freq	F(4,32) = 6.635, p = 0.0005	F(5,40) = 2.486, p = 0.0473
G - LP Firing Rate	F(4,32) = 36.072, p < 0.0001	F(5,40) = 26.509, p < 0.0001

	Paired Samples T-Tests with Bonferroni Correction			
Measure	**pH 5.5**	**pH 6.1**	**pH 6.7**	**pH 7.2**
B - PD Min V_m	t(14) = -16.836, p < 0.0001	t(14) = -4.575, p = 0.0073	t(14) = -2.454, p = 0.1587	t(14) = -2.823, p = 0.0896
C - LP Min V_m				
D - PD Spike Amp	t(14) = 7.664, p = 0.0002	t(14) = 3.087, p = 0.0598	t(14) = 2.226, p = 0.2265	t(14) = 1.179, p = 1.0883
E - LP Spike Amp	t(14) = 4.759, p = 0.0057	t(14) = 3.318, p = 0.0423	t(14) = 1.128, p = 1.1677	t(14) = 2.291, p = 0.2048
F - PD Burst Freq	t(14) = 4.429, p = 0.0088	t(14) = -2.908, p = 0.0786	t(14) = -1.509, p = 0.6788	t(14) = -0.975, p = 1.4331
G - LP Firing Rate	t(14) = 14.188, p < 0.0001	t(14) = 5.979, p = 0.0013	t(14) = 2.726, p = 0.1040	t(14) = 0.867, p = 1.6453

	Paired Samples T-Tests with Bonferroni Correction				
Measure	**pH 8.3**	**pH 8.8**	**pH 9.3**	**pH 9.8**	**pH 10.4**
B - PD Min V_m					
C - LP Min V_m	t(14) = 2.828, p = 0.1112	t(14) = 4.262, p = 0.0138	t(14) = 5.670, p = 0.0024	t(14) = 6.872, p = 0.0006	t(14) = 10.035, p < 0.0001
D - PD Spike Amp					
E - LP Spike Amp	t(14) = 0.537, p = 3.0285	t(14) = -1.925, p = 0.4521	t(14) = 2.304, p = 0.2507	t(14) = 1.768, p = 0.5750	t(14) = 1.658, p = 0.6794
F - PD Burst Freq	t(14) = -0.935, p = 1.8851	t(14) = -0.426, p = 3.4058	t(14) = 2.230, p = 0.2815	t(14) = 0.652, p = 2.6625	t(14) = 1.114, p = 1.4879
G - LP Firing Rate	t(14) = -7.134, p = 0.0005	t(14) = 0.350, p = 3.6770	t(14) = 3.753, p = 0.0280	t(14) = 4.899, p = 0.0060	t(14) = 8.277, p = 0.0002

Figure 4—figure supplement 1. Statistical analysis of the effects of pH on isolated PD and LP neurons.

The main effects of acid and base protocols on six measures of the activity of isolated LP and PD neurons were assessed. Univariate Type III Repeated-Measures Analysis of Variance (ANOVA) tests were performed separately for both acid and base step protocols. Post-hoc paired samples t-tests with Bonferroni correction were performed for each pH step against its respective control, the pH 7.8 condition immediately prior to the step protocol.

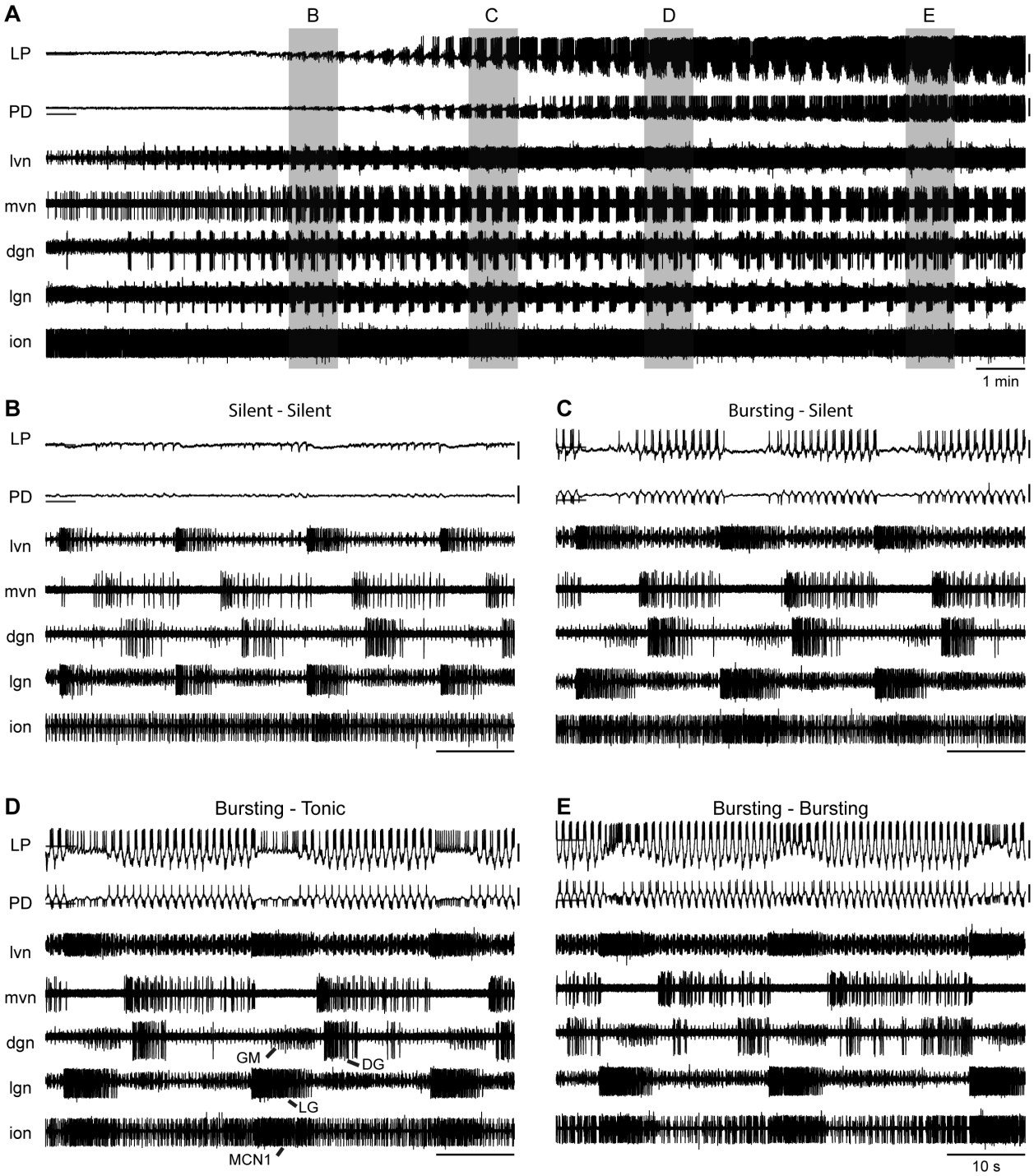

Figure 5. Rhythmic gastric-like activity upon recovery from extreme acid.
(A) 20 minutes of recording are shown from an example experiment where the ganglion had become silent at pH 5.5 and began recovering rhythmic activity in control pH 7.8 saline. Intracellular recordings from LP and PD neurons and extracellular recordings from five nerves – *lvn*, *mvn*, *dgn*, *lgn*, and *ion* – are displayed. Horizontal lines indicate a reference membrane potential of -40 mV; vertical lines indicate a scale of 10 mV. Gray boxes correspond to the one-minute snapshots enlarged in subsequent panels respective to time. **(B-E)** Titles describe the pyloric neuron activity during and between LG bursts.

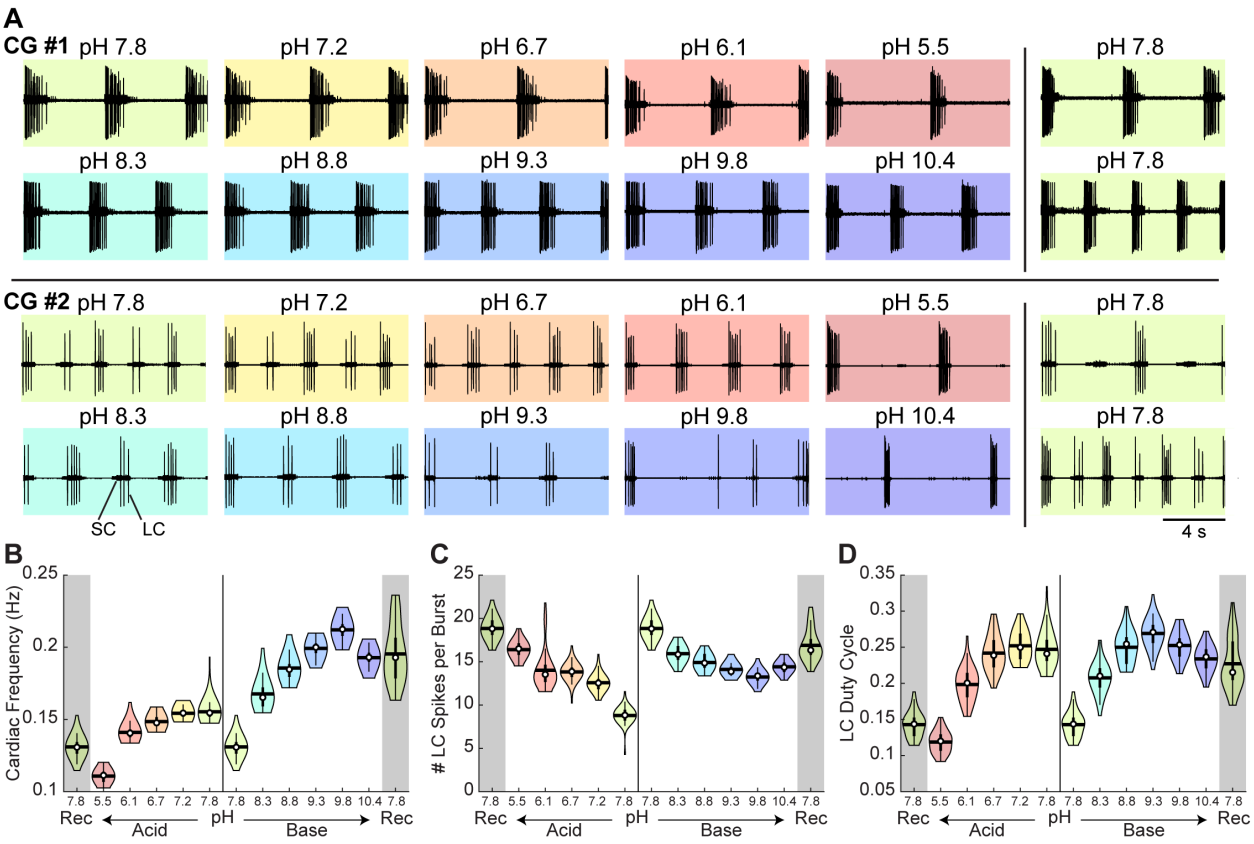

Figure 6. Robust and variable cardiac rhythm activity across pH.
(A) Two example cardiac ganglion experiments with an acid-first protocol. Each colored box displays 12 seconds of extracellular recordings of the trunk taken from the last minute of each pH condition. Small Cell (SC) and Large Cell (LC) activity is visible. Each experiment can be read left to right then top to bottom in chronological order. **(B)** Cardiac frequency, **(C)** number of LC spikes per burst, and **(D)** LC duty cycle were calculated for CG #1 for each pH step. Violin plots show the KDE distribution, mean, median, IQR, and 95% CI for each measure across pH conditions. Recoveries from acid and base are displayed in the shaded gray regions on the far ends of each plot.

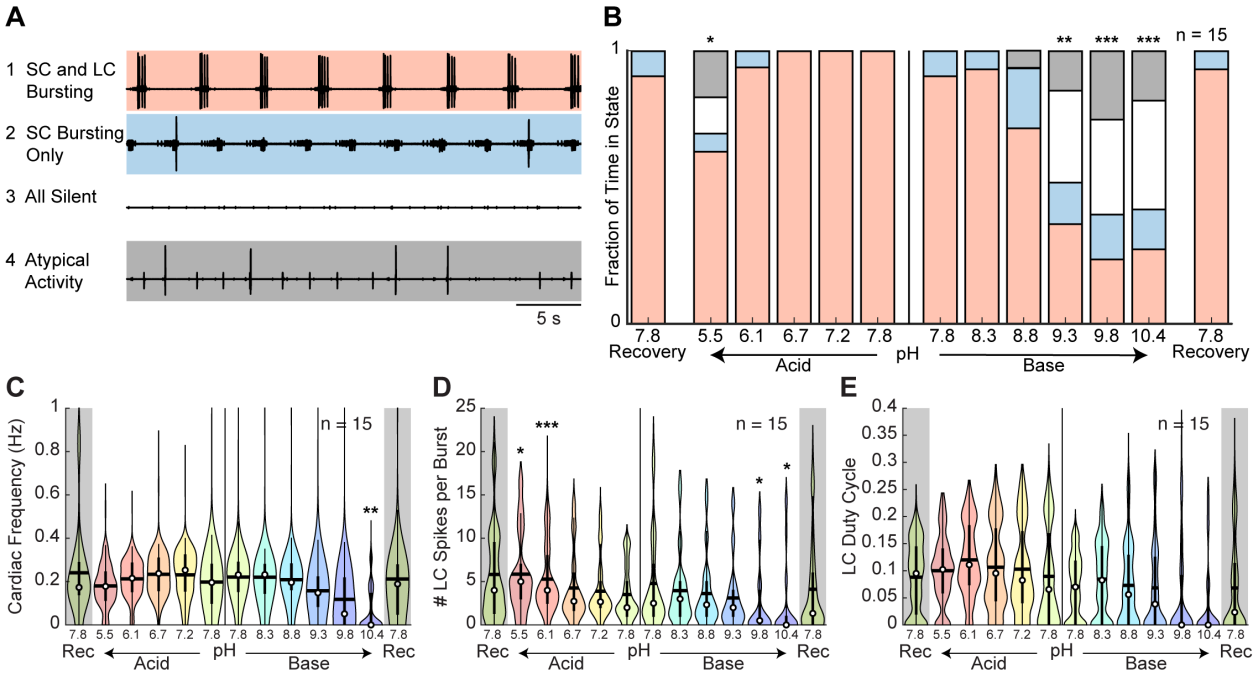

Figure 7. Characteristics of cardiac rhythm activity across pH.
(A) Four states were defined to characterize cardiac rhythm activity. Examples of activity for each state are given. **(B)** Stacked bars give the mean fraction of time that all 15 preparations spent in each state for each pH step. **(C)** Cardiac rhythm frequency, **(D)** number of LC spikes per burst, and **(E)** LC duty cycle were calculated and pooled across all CG preparations for each pH step. Violin plots show the KDE distribution, mean, median, IQR, and 95% CI for each measure across pH conditions. Recoveries from acid and base are displayed in the shaded gray regions on the far ends of each plot. Asterisks denote statistical significance revealed by paired samples t-tests with Bonferroni correction (*p<0.05; **p<0.01; ***p<0.001).

	One-Way Repeated Measures ANOVA	
Measure	**Acid**	**Base**
C - Time Rhythmic	F(4,56) = 7.458, p < 0.0001	F(5,70) = 22.496, p < 0.0001
D - Cardiac Freq	F(4,56) = 4.590, p = 0.0028	F(5,70) = 10.909, p < 0.0001
E - LC Spikes/Burst	F(4,56) = 8.094, p < 0.0001	F(5,70) = 6.675, p < 0.0001
F - LC Duty Cycle	F(4,56) = 1.709, p = 0.1609	F(5,70) = 2.714, p = 0.0267

	Paired Samples T-Tests with Bonferroni Correction			
Measure	**pH 5.5**	**pH 6.1**	**pH 6.7**	**pH 7.2**
C - Time Rhythmic	t(14) = 3.009, p = 0.0375	t(14) = 1.000, p = 1.3371	identical data	identical data
D - Cardiac Freq	t(14) = 0.792, p = 1.7661	t(14) = -0.895, p = 1.5439	t(14) = -1.985, p = 0.2684	t(14) = -1.925, p = 0.2990
E - LC Spikes/Burst	t(14) = -3.176, p = 0.0269	t(14) = -5.014, p = 0.0008	t(14) = -1.754, p = 0.4055	t(14) = -1.126, p = 1.1157
F - LC Duty Cycle				

	Paired Samples T-Tests with Bonferroni Correction				
Measure	**pH 8.3**	**pH 8.8**	**pH 9.3**	**pH 9.8**	**pH 10.4**
C - Time Rhythmic	t(14) = -1.000, p = 1.6714	t(14) = 1.920, p = 0.3774	t(14) = 4.592, p = 0.0021	t(14) = 5.806, p = 0.0002	t(14) = 6.057, p = 0.0001
D - Cardiac Freq	t(14) = 0.026, p = 4.8976	t(14) = 0.696, p = 2.4889	t(14) = 2.502, p = 0.1269	t(14) = 2.750, p = 0.0782	t(14) = 4.554, p = 0.0023
E - LC Spikes/Burst	t(14) = 1.446, p = 0.8508	t(14) = 1.591, p = 0.6693	t(14) = 2.258, p = 0.2023	t(14) = 3.236, p = 0.0299	t(14) = 3.089, p = 0.0400
F - LC Duty Cycle	t(14) = -1.133, p = 1.3809	t(14) = -0.159, p = 4.3804	t(14) = 0.143, p = 4.4424	t(14) = 1.152, p = 1.3435	t(14) = 1.654, p = 0.6019

Figure 7—figure supplement 1. Statistical analysis of the effects of pH on the cardiac rhythm.

The main effects of acid and base protocols on four measures of the activity of the cardiac rhythm were assessed. Univariate Type III Repeated-Measures Analysis of Variance (ANOVA) tests were performed separately for both acid and base step protocols. Post-hoc paired samples t-tests with Bonferroni correction were performed for each pH step against its respective control, the pH 7.8 condition immediately prior to the step protocol.

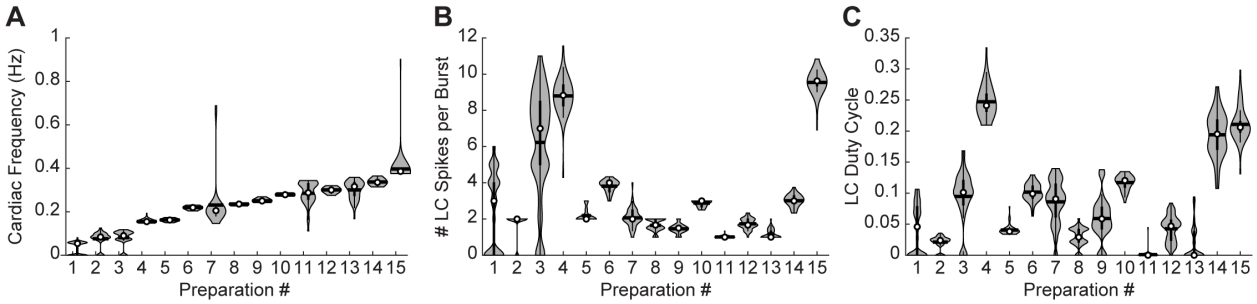

Figure 7—figure supplement 2. Variability of cardiac rhythm activity at control pH. **(A)** Cardiac rhythm frequency, **(B)** number of LC spikes per burst, and **(C)** LC duty cycle were calculated for each CG preparation for the last eight minutes in control pH 7.8. Violin plots show the KDE distribution, mean, median, IQR, and 95% CI for each measure across preparations. Preparations are consistent across plots and sorted in order of increasing frequency.

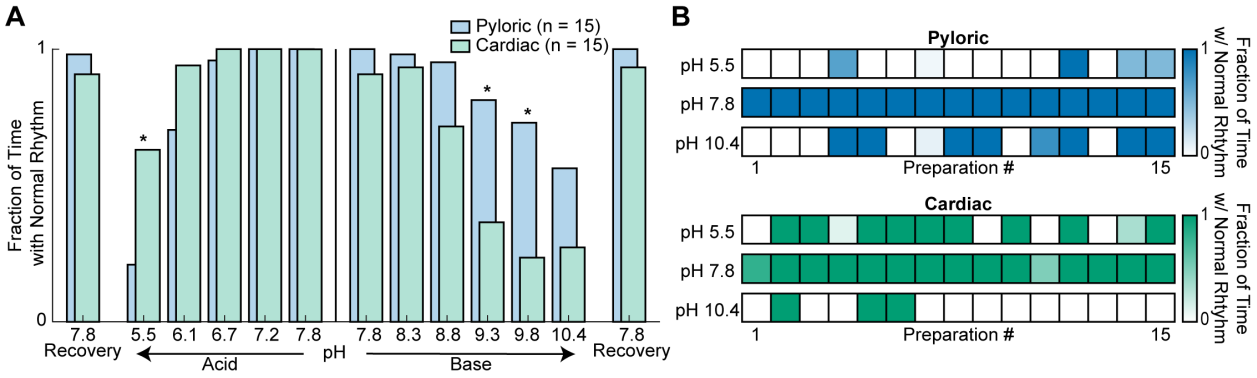

Figure 8. Rhythmicity of the cardiac and pyloric rhythms compared across pH. **(A)** Mean fraction of time that both the pyloric (blue) and cardiac (green) rhythms displayed normal activity is plotted as a function of pH. Differences between the activity of the two rhythms were analyzed by independent samples t-tests at each pH. Recovery from acid and base are displayed on the far ends of the plot. Asterisks denote statistical significance with Bonferroni correction (*p<0.05; **p<0.01; ***p<0.001). **(B)** Rhythmicity of individual animal preparations is plotted for extreme acid (pH 5.5), control (pH 7.8) and extreme base (pH 10.4) saline conditions. Each column of boxes represents a single preparation, with position across conditions remaining constant. The saturation of each box represents the mean fraction of time with a normal rhythm as indicated by the color bars on the right.

	Two-Way Mixed Measures ANOVA	
Effect	**Acid**	**Base**
Ganglion	F(1,28) = 9.043, p = 0.0055	F(1,28) = 8.788, p = 0.0061
pH	F(4,112) = 7.226, p < 0.0001	F(5,140) = 23.734, p < 0.0001
Ganglion x pH	F(4,112) = 5.392, p = 0.0005	F(5,140) = 3.530, p = 0.0049

	Independent Samples T-Tests with Bonferroni Correction			
Measure	**pH 5.5**	**pH 6.1**	**pH 6.7**	**pH 7.2**
Time Rhythmic	t(14) = 3.034, p = 0.0225	t(14) = 1.839, p = 0.3198	t(14) = 1.000, p = 1.3371	identical data

	Independent Samples T-Tests with Bonferroni Correction				
Measure	**pH 8.3**	**pH 8.8**	**pH 9.3**	**pH 9.8**	**pH 10.4**
Time Rhythmic	t(14) = -0.680, p = 2.5301	t(14) = -2.049, p = 0.2698	t(14) = -3.052, p = 0.0253	t(14) = -3.098, p = 0.0221	t(14) = -1.858, p = 0.3696

Figure 8—figure supplement 1. Statistical analysis of the differential effects of pH on the pyloric and cardiac rhythms.
The main effects of ganglion and pH and their interaction during both acid and base protocols on the fraction of time rhythmic of both the pyloric and cardiac rhythms were assessed. Multivariate Type III Mixed-Measures Analysis of Variance (ANOVA) tests were performed separately for acid and base step protocols. Post-hoc independent samples t-tests with Bonferroni correction were performed to compare rhythmicity of stomatogastric and cardiac preparations at each pH step.